



CrossMark
click for updates

Cite this: *RSC Adv.*, 2015, 5, 3619

An efficient robust fluorite $\text{CeZrO}_{4-\delta}$ oxide catalyst for the eco-benign synthesis of styrene

Kaliyappan Periyasamy,^a Venugopalan T. Aswathy,^a Venugopal Ashok kumar,^a Marimuthu Manikandan,^a Rakesh Shukla,^b Avesh K. Tyagi^{*b} and Thirumalaiswamy Raja^{*a}

In this work, we have reported CeO_2 , ZrO_2 , physically mixed (PH)- $\text{CeO}_2/\text{ZrO}_2$ and fluorite $\text{CeZrO}_{4-\delta}$ oxides and their catalytic activities for the oxidative dehydrogenation (ODH) of ethyl benzene (EB) to styrene (ST) using molecular oxygen, air and carbon dioxide as oxidants. The catalysts were prepared by a gel-combustion method followed by calcination at 600 °C for 6 h and subjected to catalytic activity measurements. All the catalysts were characterized and studied by various physicochemical methods. The reaction parameters were varied systematically such as different catalysts, oxidants, temperatures, EB flow and oxidant flow. $\text{CeZrO}_{4-\delta}$ accounted for a 47% styrene yield for 72 h without any significant deactivation under optimized reaction conditions. A thorough analysis of the spent catalysts demonstrated the robustness of the catalyst for this reaction under different oxidants and reaction conditions. Pristine CeO_2 deactivated easily and the activity decreased with time on stream of the reaction.

Received 14th October 2014
Accepted 2nd December 2014

DOI: 10.1039/c4ra12355g

www.rsc.org/advances

Introduction

Ethyl benzene (EB) to styrene (ST) is a commercially important pathway in polymer and petrochemical industries. Styrene is an important monomer for the production of polystyrene, plastics, styrene-acrylonitrile, styrene butadiene latex and other copolymers.¹ Commercially styrene is produced by dehydrogenation of ethyl benzene using potassium promoted hematite catalysts with superheated steam at 700 °C.² This dehydrogenation reaction is a highly endothermic process and the stringent reaction conditions are the main drawback. To overcome this, oxidative dehydrogenation (ODH) of EB is an alternative process for the production of ST to realize an exothermic reaction and shift entirely the equilibrium towards the desired product formation and to carry out the reaction at lower temperature. ODH of EB to ST is one of the most industrially important reactions which possess the challenge of tailoring of suitable catalysts and relatively non stringent reaction conditions. Use of soft oxidants like CO_2 ,^{3,4} N_2O ,^{5,6} O_2 ⁷ and air^{8,9} are environmentally benign process. Venugopal *et al.* had reported that the ceria supported hydrotalcite catalyst has maximum conversion for ethyl benzene using oxygen as an oxidant.⁷ They also reported that ceria loading is directly proportional to the conversion and selectivity.⁷ Reddy *et al.* carried out ODH of EB using air over $\text{V}_2\text{O}_5/\text{Ce}_x\text{Zr}_{1-x}\text{O}_2/\text{SiO}_2$ catalysts⁸ and also they

investigated the EB to ST conversion using air as oxidant on $\text{CeO}_2/\text{Al}_2\text{O}_3$ and $\text{V}_2\text{O}_5/\text{CeO}_2/\text{Al}_2\text{O}_3$ as catalysts.¹⁰ Xiao *et al.* have reported the ODH of EB using hierarchical porous carbon spheres using molecular oxygen giving around 43% conversion.¹¹ Takehira and co-workers were reported ODH of EB using CO_2 and O_2 over Mg-Fe-Al mixed oxide derived hydrotalcite catalyst.¹² Vansant *et al.* have reported dehydrogenation of EB using N_2O over transition metals supported on mesoporous silica materials where they found Fe^{3+} is active for EB conversion.⁶

Ceria is well known for its redox properties¹³ and oxygen storage capacity, which is used in many catalytic reactions and three way catalyst.^{14,15} Fan *et al.* have reported mesostructured ceria which shows 34% conversion and 87% selectivity in EB conversion.¹⁶ Pure ceria shows low catalytic activity at higher temperatures because of its poor thermal stability.^{10,17} To overcome these disadvantages, ceria is incorporated in oxides and component of mixed oxide catalysts which shows improved activity and thermal stability.⁷ Ceria-based mixed oxide catalysts are widely used in many organic reactions.^{18,19} Zirconia has good oxygen storage capacity and thermal stability. When zirconia is incorporated in ceria lattice it enhances the oxygen storage capacity²⁰ and thermal stability.^{20,21} Di Monte *et al.* reported that ceria-zirconia mixed oxide shows high redox property and thermal stability in heterogeneous catalysis.²²

Herein, we reported the use of a $\text{CeZrO}_{4-\delta}$ as catalyst for the industrially important oxidative dehydrogenation of EB to ST. We have prepared $\text{CeZrO}_{4-\delta}$ with fluorite structure, CeO_2 and ZrO_2 by gel-combustion method, while PH- $\text{CeO}_2/\text{ZrO}_2$ was prepared by physical mixture method. These catalysts were

^aCatalysis Division, CSIR-National Chemical Laboratory, Dr Homi Bhabha Road, Pune – 411 008, India. E-mail: t.raja@ncl.res.in; Tel: +91-020-25902006

^bChemistry Division, Bhabha Atomic Research Centre, Mumbai – 400 085, India. E-mail: aktyagi@barc.gov.in; Tel: +91-022-25595330

subjected to XRD, HRTEM, Raman analysis, APPEs, TGA and N_2 adsorption techniques.

Experimental section

Catalyst preparation

To achieve better powder properties for catalysis, instead of the stoichiometric amount of oxidant-to-fuel ratio reported, a fuel-deficient ratio was selected in this case. All catalysts were prepared by gel-combustion method. Cerium(III) nitrate (Alfa Aesar), zirconyl(IV) nitrate (Loba Chemie) and glycine as fuel (Merck) were used as precursor for catalyst synthesis. Calculated amount of standard solution of zirconyl nitrate and cerium nitrate were dissolved in distilled water. To this solution, glycine (60% fuel deficient ratio *i.e.* for 1 mmol of cerium nitrate and zirconyl nitrate each, 2 mmol of glycine) was added followed by evaporation near to dryness on a hot plate to form a transparent colorless gel. On further heating on the hot plate, the gel undergoes auto-ignition to form a fluffy mass. The obtained powder was calcined at 600 °C for 6 hours. We used cerium nitrate as a precursor for pure ceria and zirconyl nitrate as a precursor for pure zirconia catalyst. Preparation method of pure ceria and pure zirconia was as same as above procedure. Above mentioned catalysts were labeled as $CeZrO_{4-\delta}$, CeO_2 and ZrO_2 . Physically mixed CeO_2/ZrO_2 catalyst was prepared by simply mixing proper amount of cerium nitrate and zirconyl nitrate together and milled. The obtained powder was calcined at 600 °C for 6 hours and the catalyst was labelled as PH- CeO_2/ZrO_2 .

The as-synthesized and spent materials were characterized by powder X-ray diffraction (PXRD) and the data were collected on PANalytical X'pert Pro dual goniometer diffractometer using $Cu\ K\alpha$ (1.5418 Å) radiation with Ni filter with a step size of 0.008° and a scan rate of 0.5° min^{-1} . Crystallite size of the catalysts was calculated by using Scherrer's formulae. Nitrogen adsorption/desorption isotherms were collected from Quantachrome USA. The samples were degassed at 250 °C for 3 h under vacuum to remove moisture and other volatiles. Surface area was calculated by Brunauer–Emmett–Teller (BET) equation from the adsorption branch. High resolution transmission electron microscopies (HR-TEM) of all materials were recorded using FEI TECNAI F30 electron microscope operating at 300 kV. Samples were powdered and dispersed in isopropanol before depositing onto a holey carbon grid. Perkin Elmer Diamond's thermogravimetry (TG) instrument was used to measure the thermal analysis of spent catalyst. Raman spectra were recorded on a Horiba JY LabRAMHR800 Raman spectrometer coupled with microscope in reflectance mode with 514 nm excitation laser source. XPS measurement for the $CeZrO_{4-\delta}$ catalyst was done by ambient pressure photoelectron spectrometer (APPEs) under UHV condition. X-rays are generated by Mg $K\alpha$ X-ray source for XPS measurement.

Catalytic activity

The catalytic evaluation was performed by using a fixed bed continuous up flow reactor (FBR) having two furnace zones at

atmospheric pressure. In a typical experiment, catalytic bed was placed at centre of the reactor which loaded with 1.0 mL of catalyst (0.9 g catalyst); above and below of the catalytic bed was filled with ceramic beads. A Inconel reactor tube with 13 mm internal diameter and 510 mm length was used to pack the catalyst. The catalyst was pelletized and sieved through the mesh size of 1.2–1.7 mm. The temperature of the reactor and catalyst bed was measured using a K-type coaxially centered thermocouple. EB feed flow of liquid hourly space velocity (LHSV) 3 h^{-1} was controlled by isocratic pump (Lab Alliance Series II) and the optimized oxygen, carbon dioxide and air flow with gas hourly space velocity (GHSV) 2400 h^{-1} was controlled by using a Brooks make mass flow controller (5890E series). The mole ratio of O_2/EB is 4. The feed flow was configured to operate up flow mode and the products were condensed using a chiller. The liquid products were analyzed using varian CP 3800 gas chromatography with HP-5 column (30 m \times 0.32 m \times 0.25 m) along with FID detector. The gas analysis was done by TCD detector with Molecular Sieve 5A. Conversion of ethyl benzene and selectivity of styrene was calculated as per procedures described elsewhere.⁷

Results and discussion

Powder X-ray diffraction

Powder X-ray Diffraction pattern for as-synthesized CeO_2 , ZrO_2 , PH- CeO_2/ZrO_2 , fresh and used $CeZrO_{4-\delta}$ catalysts are shown in Fig. 1. Powder X-ray diffraction pattern of $CeZrO_{4-\delta}$ catalyst calcined at 600 °C shows seven major peaks (111), (200), (220), (311), (222), (400) and (331) at 29.1°, 33.6°, 48.5°, 57.6°, 60.2°, 71.2° and 78.5° respectively which corresponds to cubic fluorite structure (JCPDS 38-1439). The weak cation ordered peaks for pyrochlore related $Ce_2Zr_2O_8$ could not be observed in the XRD.²³ The absence of cation ordering may be explained as follows. The fuel-deficient ratio was selected for the gel-combustion reaction, the exothermicity in the reaction was low and the heat generated was not sufficient enough for the formation of cation ordered form of this compound. Probably this could be the main reason to obtain $CeZrO_{4-\delta}$ instead of cation ordered $Ce_2Zr_2O_8$. From the most intense (111) peak at $2\theta = 29.1^\circ$

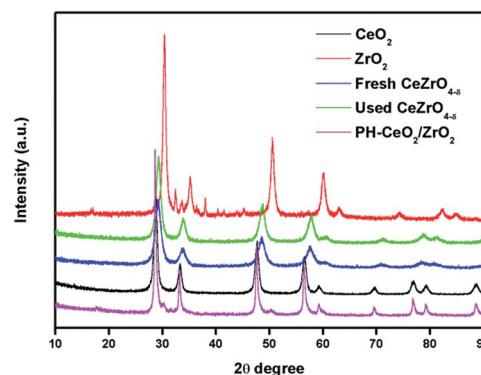


Fig. 1 Powder X-ray diffraction pattern of CeO_2 , ZrO_2 , PH- CeO_2/ZrO_2 , fresh and used $CeZrO_{4-\delta}$ catalysts.

Table 1 Surface area and crystallite size of as-prepared catalysts

S. no.	Sample	Crystallite size ^a (nm)	Surface area (m ² g ⁻¹)	Pore volume ^b (cc g ⁻¹)
1	CeZrO _{4-δ}	6.2	31	0.18
2	CeO ₂	11.0	37	0.16
3	ZrO ₂	13.5	23	0.14
4	PH-CeO ₂ /ZrO ₂	28.8	22	0.16

^a Average crystallite size calculated from Scherrer equation. ^b Pore volume from BET surface area.

FWHM value was taken and the crystallite size was calculated. The crystallite size for CeZrO_{4-δ} catalyst is ~6 nm. Surface area and crystallite size of as prepared catalysts are given in Table 1.

Surface area depends on crystallite size *i.e.*, when the size of the particles decreases surface area increases and *vice versa*. Surface area of pure ceria was 37 m² g⁻¹, which is higher compare to other catalysts. When zirconia is incorporated into the ceria lattice, surface area is decreased to 31 m² g⁻¹ which may be due to insertion of zirconia into ceria lattice and increase in crystallinity leads to decrease in the specific surface area.²⁴ Pure zirconia and physical mixture of CeO₂/ZrO₂ shows low surface area compared to other catalysts.

Raman spectroscopy

Raman spectra for as-prepared ceria catalyst shows only one high intensity peak at 465 cm⁻¹ corresponds to typical Raman active cubic fluorite F_{2g} CeO₂. For zirconia, Raman spectrum shows six peaks corresponds to tetragonal phase of ZrO₂.²⁵ Typical Raman spectrum of CeO₂, ZrO₂, fresh and used CeZrO_{4-δ} catalysts are shown in Fig. 2. Raman spectra of CeZrO_{4-δ} catalyst shows a high intense peak at 473 cm⁻¹ and two broad shoulder peaks at 310 and 620 cm⁻¹. There is no tetragonal phase for zirconia in CeZrO_{4-δ} catalyst which means that the ceria and zirconia form a solid solution and stabilize in the single phase fluorite structure. The absence of Raman shift of the pyrochlore modes also confirms the stabilization of fluorite phase, which is in accordance with XRD data. The strong intense peak at 465 cm⁻¹ (inset) corresponds to ceria. The progressive shift of ceria peak from 465 to 473 cm⁻¹ is due

to the cell contraction attributed to zirconia incorporation in the ceria lattice.²⁶ This is further confirmed as there is decrease of lattice parameter of the product compared to that of parent ceria. This blue shift indicated the change in chemical interaction and lattice parameters possibly due to the insertion of Zr in ceria lattice.^{27,28} The peak at 310 cm⁻¹ shows change in the position of oxygen atom from their ideal fluorite structure. The broad and weak peak at 620 cm⁻¹ attributes to Raman inactive lattice oxygen mode in CeZrO_{4-δ} catalyst. The appearance of this peak is due to the presence of oxygen vacancy in the fluorite phase which causes defective sites in Ce–Zr oxides for the activity of the catalyst. Full width at half maximum (FWHM) of F_{2g} peak of ceria in the mixed oxide can be used to measure the oxygen vacancies in the catalyst. An increasing amount of Zr incorporation in CeO₂ lattice along with increasing oxygen vacancies are possible reasons for the above changes in Raman spectra.

Transmission electron microscopy (TEM)

Morphology and textural properties of the CeZrO_{4-δ} catalyst has been studied by HR-TEM. Average size of the crystallites was apparently reduced, and what cause this size reduction is unknown. HRTEM images of the CeZrO_{4-δ} catalyst at low and high resolution are shown in Fig. 3. The particle size was measured for CeZrO_{4-δ} catalyst; it shows 6 ± 1 nm which is in good agreement with XRD data. Selected Area Electron Diffraction (SAED) confirmed the crystalline nature of the

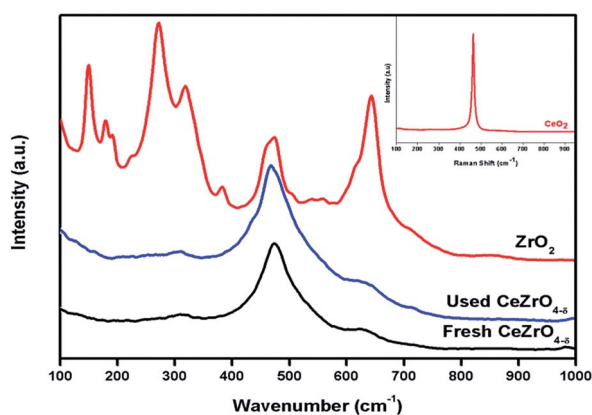


Fig. 2 Raman spectroscopy of the CeO₂, ZrO₂, fresh and used CeZrO_{4-δ} catalysts.

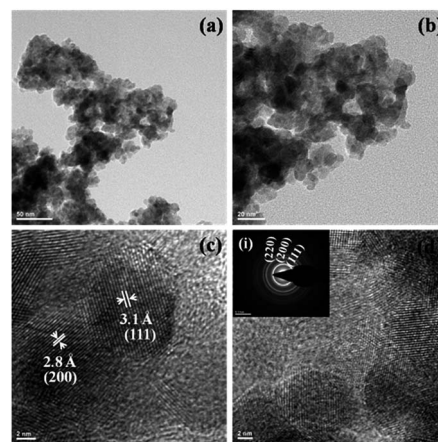


Fig. 3 TEM images of the CeZrO_{4-δ} fresh catalyst calcined at 600 °C. (a and b) Low resolution and (c and d) high resolution (inset: SAED pattern).

CeZrO_{4-δ} catalyst which is shown in inset image in Fig. 3d(i). The *d*-spacing value of ~3.1 Å and ~2.8 Å corresponds to the (111) and (200) planes respectively for CeZrO_{4-δ} catalyst. These *d*-spacing values further confirm the fluorite nature of CeZrO_{4-δ} sample.

A disordered mesoporous structure was observed for CeZrO_{4-δ} catalyst. HRTEM image shows the majority of lattice fringes corresponding to ceria-zirconia (111) facets (*d* = 0.31 nm) of cubic fluorite structure. These observations are in excellent agreement with XRD results. Disordered mesoporous nature has further advantages like low diffusional barriers, since the depth of mesopores are minimum to a few nanometres, unlike several hundred nanometres in conventional ordered mesoporous materials, like MCM-41 and SBA-15.²⁹ This type of interface is crucial for the transport of reactants, especially oxygen, across the interface from ceria to zirconia, possibly through reverse spill-over phenomenon.

To confirm the stability of CeZrO_{4-δ} catalyst, HRTEM studies have done for used catalyst (72 hours time on stream) and are shown in Fig. 4. It clearly shows that there is no change in morphology of the catalyst after 72 hours reaction at optimized reaction conditions. Some amount of carbon is deposited on the surface of the catalyst is clearly observed in HRTEM image. TGA confirms that the carbon deposited on the catalyst is around 3.1%.

X-ray photoelectron spectroscopy (XPS)

To understand the surface of the catalyst and oxidation state of CeZrO_{4-δ} catalyst, it was subjected to X-ray photoelectron spectroscopy (XPS). Ceria has two oxidation states such as +3 and +4; it switches over the oxidation state, which causes redox property of ceria. Fig. 5 shows the XPS spectra of Ce 3d level and unveils the presence of both Ce⁴⁺ and Ce³⁺ peaks where Ce⁴⁺ shows Ce 3d_{5/2} and Ce 3d_{3/2} peaks at 900.8 eV(u), 907.2 eV(u''), 916.7 eV(u''') and 882.4 eV(v), 888.8 eV(v''), 898.1 eV(v''') respectively.^{30,31} For Ce³⁺, it has four peaks at 903.7 eV(u'), 884.7 eV(v'), 899.2 eV(u₀), and 880.1 eV(v₀).³⁰⁻³² In Ce 3d spectra of CeZrO_{4-δ} catalyst similar binding energy for all peaks are compared with pure ceria. But the intensity of Ce³⁺ was higher than pure ceria, which shows more defective sites in CeZrO_{4-δ} catalysts. Ce³⁺ and Ce⁴⁺ oxidation states were confirmed by Ce 3d spectra. Incorporation of zirconia into ceria increases the

redox property of ceria and more defective sites are generated, which favoured for ODH of EB to ST.

XPS spectrum of Zr 3d and O 1s are shown in Fig. 6. In pure ceria, the binding energy of oxygen 1s peaks at 528.6, 528.8, 529.6 and 530.1 eV were observed which are in agreement with reported values of literature.^{29,33} For zirconia, the binding energy of oxygen 1s spectra peak at 530.6 eV is also congruent with literature.³⁴ In CeZrO_{4-δ} catalyst, only two O 1s peaks were observed at 529.7 and 531.1 eV which corresponds to lattice oxygen and surface hydroxyl group respectively.^{7,35} Fig. 6(a) shows zirconium 3d spectra with most prominent peak at 181.1 eV corresponding to Zr 3d_{5/2} and low intense peak at 184.2 eV corresponding to Zr 3d_{3/2} peak, it clearly indicates that zirconia is in Zr⁴⁺ oxidation state.³⁶

Catalytic activity

Effect of temperature. Temperature is an important governing parameter for EB to ST conversion. Although EB conversion is directly proportional to increase in reaction temperature in some instances above an optimum temperature, combustion is always favoured and unavoidable; this leads to decrease in the overall ST yield. To optimize reaction temperature for ST yield, studies were carried out in different temperature range between 400 °C to 600 °C. At different temperatures, the catalytic activity of CeZrO_{4-δ} catalyst differs, with fixed flow of EB and oxygen. Fig. 7 shows the temperature profile of ODH of EB. Maximum yield of ST is observed at 550 °C with stable catalytic activity. Over 550 °C the combustion was mostly

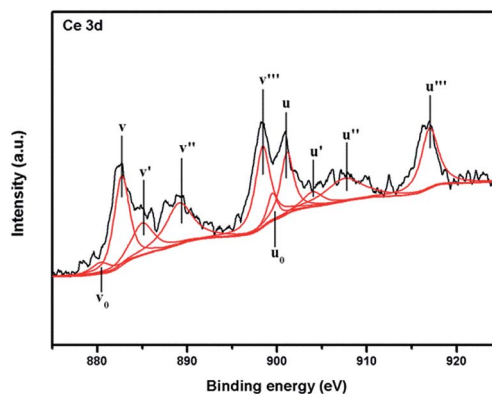


Fig. 5 Ce 3d spectra of CeZrO_{4-δ} catalyst.

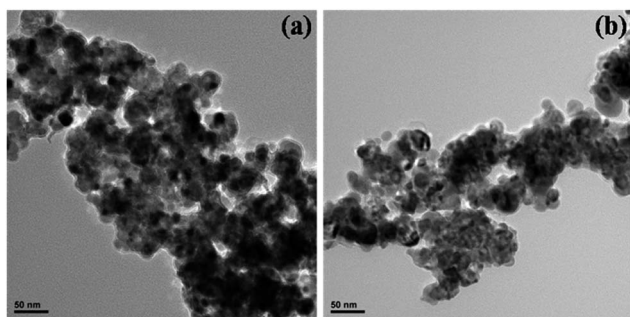


Fig. 4 TEM images of the used CeZrO_{4-δ} catalyst (a and b) at optimized reaction conditions after 72 h TOS.

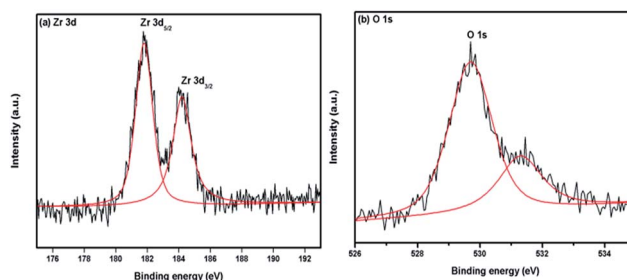


Fig. 6 XPS spectrum of CeZrO_{4-δ} catalyst (a) Zr 3d and (b) O 1s.

favoured. Increase in temperature increased the conversion of EB in certain extent but the selectivity rapidly decreases from 91% to 76%. Decrease in selectivity was observed above 550 °C, this may be due to the formation of undesired by-products like CO_x , and other products. Maximum conversion of 40% and selectivity of 93% was observed at 550 °C with stable catalytic activity. Hence, 550 °C was taken as the optimum temperature for obtaining a maximum yield of styrene.

Influence of contact time. To exploit the effect of contact time between reactants and catalytic active sites, reaction was carried at with different EB flow at optimized temperature and fixed oxygen flow. EB conversion and ST selectivity of the $\text{CeZrO}_{4-\delta}$ catalyst at different reactant flow is shown in Fig. 8. Three different EB flows of LHSV 2, 3 and 5 h^{-1} were investigated. While increasing EB flow, there is a constant increase in the conversion of EB but decrease in ST selectivity. We have also observed that lower EB flow (LHSV 2 h^{-1}), has 37% conversion of EB and at LHSV 3 h^{-1} the conversion increased up to 50%. Further increase in EB flow (LHSV 5 h^{-1}), both the conversion and selectivity decreased, which might be due to shorter

resident time of reactants over the catalytic active sites. Maximum EB conversion of 50% and ST selectivity of 93% is observed with EB flow LHSV 3 h^{-1} with the function of time. LHSV 3 h^{-1} was taken as the optimum flow for EB based on the above mentioned trend.

Effect of oxidant flow. Catalytic activity of the ODH is also influenced by the oxidant flow. To understand the impact of oxidant flow (O_2) on catalytic activity, we carried out with different flow rate of oxygen (GHSV 600 h^{-1} , 1200 h^{-1} , 2400 h^{-1} and 3600 h^{-1}). Fig. 9 shows effect of oxygen flow in the ODH of EB with different oxidant flow rates, at optimized temperature and EB flow. Ceria-zirconia catalyst has good oxygen storage capacity and high thermal stability. Here, we are reporting this class of pyrochlore related catalyst for the first time in ODH and it shows the best activity than other catalysts. In this ODH reaction, formation of thin layer of coke in initial hours plays important role in increasing the catalytic activity.^{37,7} We observed the maximum conversion of EB and selectivity of styrene is 50% and 93% at GHSV 2400 h^{-1} respectively. Conversion of EB and selectivity towards styrene is increased with increase in oxidant flow rate up to GHSV 2400 h^{-1} . Further increase in oxidant flow (GHSV 3600 h^{-1}), conversion of EB and selectivity towards styrene is decreased rapidly; it may be due to over oxidation which leads to CO_x , water and other unwanted side products. Minimum conversion of EB and selectivity towards styrene is observed in lower oxidant flow of GHSV 600 h^{-1} it may be due to inadequate oxidant. GHSV 2400 h^{-1} with respect to oxidant flow was considered as the optimum flow to achieve maximum yield of styrene.

In order to study the stability of the catalyst with constant yield of ST by longer time (72 h) on stream (TOS) was performed under optimized reaction conditions *i.e.* 550 °C, LHSV 3 h^{-1} with respect to EB and GHSV 2400 h^{-1} with respect to oxygen at atmospheric pressure. The activity of the catalyst remains same for longer duration as in optimized conditions and the stability of the catalyst remains stable with only very small decrease in conversion even after 72 h. Fig. 10 shows 72 hours time on stream of $\text{CeZrO}_{4-\delta}$ catalyst at optimized reaction condition for

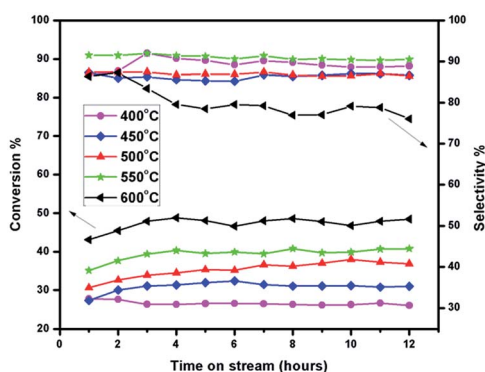


Fig. 7 EB conversion and styrene selectivity of the $\text{CeZrO}_{4-\delta}$ catalyst on oxidative dehydrogenation of EB at different temperatures (reaction conditions: 400–600 °C, LHSV 3 h^{-1} with respect to EB, GHSV 1200 h^{-1} with respect to oxygen, 1 atmosphere pressure, 1 mL catalyst).

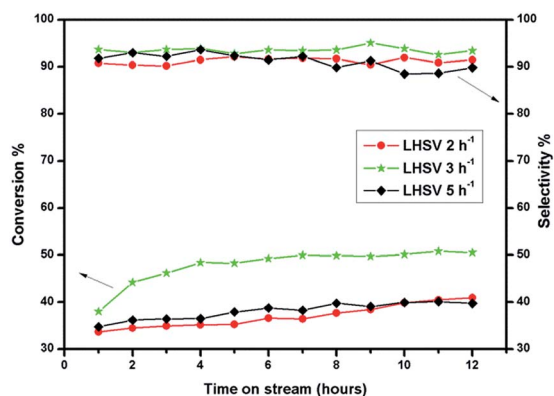


Fig. 8 EB conversion and styrene selectivity of the $\text{CeZrO}_{4-\delta}$ catalyst on oxidative dehydrogenation of EB at various contact time (reaction conditions: 550 °C, GHSV 2400 h^{-1} with respect to oxygen, LHSV 3–5 h^{-1} with respect to EB, 1 atmosphere pressure, 1 mL catalyst).

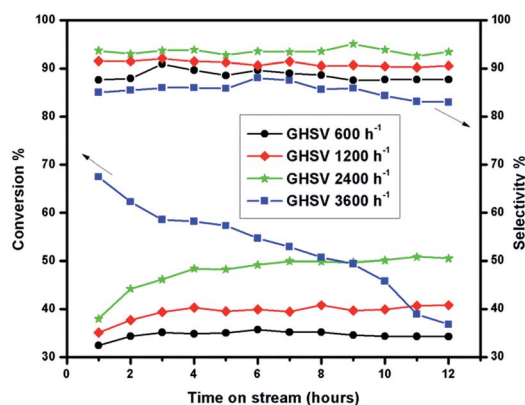


Fig. 9 EB conversion and styrene selectivity of the $\text{CeZrO}_{4-\delta}$ catalyst on oxidative dehydrogenation of EB at various oxidant flows (reaction condition: 550 °C, LHSV 3 h^{-1} with respect to EB, GHSV 600–3600 h^{-1} with respect to oxygen, 1 atmosphere pressure, 1 mL catalyst).

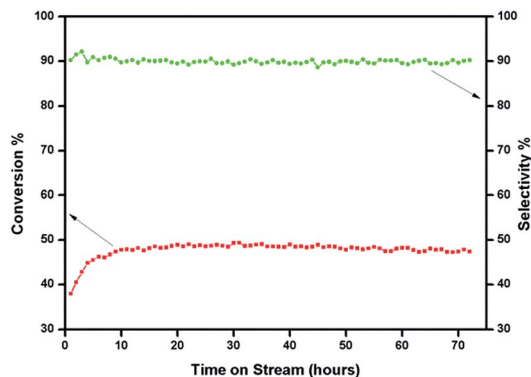


Fig. 10 72 hours TOS study of oxidative dehydrogenation of EB to ST over $\text{CeZrO}_{4-\delta}$ catalyst (reaction conditions: 550°C , LHSV 3 h^{-1} with respect to EB, GHSV 2400 h^{-1} with respect to oxygen, 1 atmosphere pressure, 1 mL catalyst).

EB to ST. Due to its better oxygen storage/release capacity, poor sinterability and fluorite $\text{CeZrO}_{4-\delta}$ phase, it showed constant catalytic activity even after 72 h. There is also no change in phase of the catalyst which is confirmed by XRD pattern as shown in Fig. 1

Impact of different phases. Fig. 11 shows the catalytic activity of CeO_2 , ZrO_2 , $\text{PH-CeO}_2/\text{ZrO}_2$ and $\text{CeZrO}_{4-\delta}$ catalyst under optimized reaction conditions on 18 hours time on stream. To know which phase is active for ODH of EB, these CeO_2 , ZrO_2 , $\text{PH-CeO}_2/\text{ZrO}_2$ and $\text{CeZrO}_{4-\delta}$ catalysts were subjected to ODH of EB reaction. CeO_2 , ZrO_2 and $\text{PH-CeO}_2/\text{ZrO}_2$ catalysts show cubic, tetragonal, cubic/tetragonal phases, respectively. $\text{CeZrO}_{4-\delta}$ adopts a fluorite structure as confirmed by XRD data. Pure ceria shows better conversion at initial time and then rapidly decreased which is usually obtained for ceria. For pure zirconia, the conversion and selectivity was low compared to other catalysts which may be due to coke formation on the catalyst. Compared to $\text{CeZrO}_{4-\delta}$ catalyst, $\text{PH-CeO}_2/\text{ZrO}_2$ catalyst shows low conversion and selectivity towards styrene.

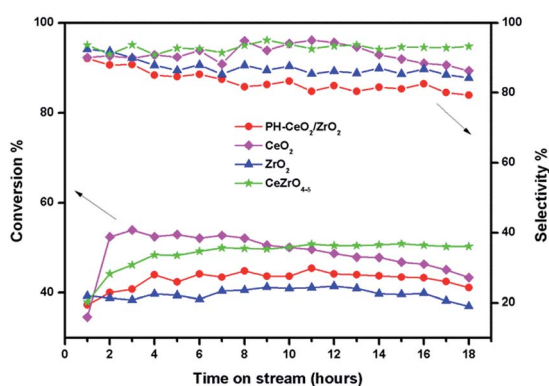


Fig. 11 EB conversion and styrene selectivity of the different catalysts on oxidative dehydrogenation of EB (reaction condition: 550°C , LHSV 3 h^{-1} with respect to EB, GHSV 2400 h^{-1} with respect to oxygen, 1 atmosphere pressure, 1 mL catalyst).

The $\text{CeZrO}_{4-\delta}$ catalyst shows maximum conversion and selectivity of 50% and 93% on 18 hours time on stream compared to other catalysts studied. Zirconia shows lowest conversion and selectivity compared to other catalysts.

In $\text{CeZrO}_{4-\delta}$ catalyst, selectivity towards styrene is highest (93%) among other catalyst. For pure ceria, zirconia and physical mixture of ceria-zirconia shows low selectivity towards styrene because of formation of by-products like benzene, toluene, styrene oxide and CO_x . Conversion and selectivity of different catalysts is shown in Table 2.

Influence of oxidants. To study the influence of participation of oxidants, the reaction was carried with and without oxidants at optimized reaction conditions which revealed the participation of lattice oxygen or oxidant. The reaction without oxidant at optimized reaction conditions shows only 23% conversion of EB and 22% yield of ST which indicates, that the lattice oxygen drives the reaction. To confirm the result, we introduced oxygen as oxidant into the reaction; the conversion and yield increased to 52% and 48% respectively (Fig. 12). It may be due to facile dissociation of molecular oxygen on the surface of the catalyst, which is further reactive towards EB to convert styrene. The removal of lattice oxygen is replenished by substituting gaseous molecular oxygen into the lattice which enhances the catalytic activity.³⁸

Table 2 Conversion and selectivity of the different catalysts on ODH of EB

Catalyst	Conversion% (EB)	Selectivity%					Yield% (ST)
		ST ^a	BZ ^b	TU ^c	SO ^d	CO _x	
CeO_2	43	86	1.5	4.2	—	8.3	36
ZrO_2	37	84	—	2.4	1.4	12.2	31
$\text{CeZrO}_{4-\delta}$	50	93	4.3	1.4	0.5	0.8	47
$\text{PH-CeO}_2/\text{ZrO}_2$	44	79	2.1	4.5	8.0	6.4	35

^a ST-styrene. ^b BZ-benzene. ^c TU-toluene. ^d SO-styrene oxide.

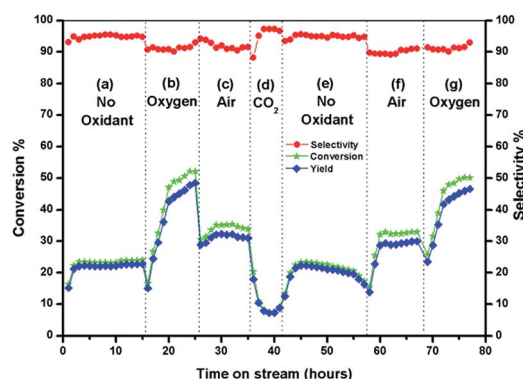


Fig. 12 Different oxidants study of oxidative dehydrogenation of EB to ST over $\text{CeZrO}_{4-\delta}$ catalyst (reaction conditions: 550°C , LHSV 3 h^{-1} with respect to EB, 1 atmosphere pressure, 1 mL catalyst). (a) Without oxidant, (b) with oxygen (GHSV 2400 h^{-1}), (c) with air (GHSV $10\ 800\text{ h}^{-1}$), (d) with carbon dioxide (GHSV 2400 h^{-1}), (e) without oxidant, (f) with air (GHSV $10\ 800\text{ h}^{-1}$), (g) with oxygen (GHSV 2400 h^{-1}).

Table 3 Effect of various oxidants on catalytic activity of CeZrO_{4-δ} for ODH of EB

Oxidant	Conversion% (EB)	Selectivity%					Yield% (ST)
		ST ^d	BZ ^e	TU ^f	SO ^g	CO _x	
Nil	23	94	4.0	2.0	—	—	22
Oxygen ^a	51	92	4.8	1.0	0.4	0.8	47
Air ^b	33	91	2.0	1.0	5.0	1.0	31
Carbon dioxide ^c	07	97	2.0	0.6	—	0.4	7

^a GHSV 2400 h⁻¹ with respect to oxygen. ^b GHSV 10 800 h⁻¹ with respect to air. ^c GHSV 2400 h⁻¹ with respect to carbon dioxide (reaction conditions: temperature 550 °C, LHSV 3 h⁻¹ with respect to EB, 1 atmosphere pressure, 1 mL catalyst). ^d ST-styrene. ^e BZ-benzene. ^f TU-toluene. ^g SO-styrene oxide.

ODH of EB was studied with soft oxidants like CO₂ and air continuously in time on stream. EB conversion and ST yield for CO₂ as oxidant were low compared to other oxidants; it may be due to coke formation or inability to activate the CO₂. There is not much replenishing of lattice oxygen by air, so air as oxidant shows less conversion than oxygen. If oxygen is used as an oxidant, replenishing of the lattice oxygen by molecular oxygen leads to enhancement in the catalytic activity which leads to maximum conversion and selectivity. Maximum EB conversion was obtained for oxygen as an oxidant. Table 3 shows the effect of various oxidants on catalytic activity of CeZrO_{4-δ} for ODH of EB.

Stable conversion and yield were obtained without oxidant upto 15 hours. After that oxygen was introduced as oxidant, conversion and yield attained maximum. Without oxidant, the conversion was only 23% which might be possibly due to minimum availability of lattice oxygen. If oxygen is introduced into reaction, conversion suddenly increases to 40% this may be ease of availability and replenishment of lattice oxygen. This catalyst shows stable conversion and yield with different oxidants up to 76 hours.

Conclusion

CeO₂, ZrO₂, CeZrO_{4-δ} and PH-CeO₂/ZrO₂ catalyst were successfully synthesized by gel-combustion and physical mixture method. Catalytic activity was performed using fixed bed continuous up flow reactor (FBR) and the catalysts were characterized by XRD, HRTEM, Raman spectroscopy, APPEs, TGA and N₂ adsorption. Fluorite CeZrO_{4-δ} catalyst shows maximum conversion of 50% towards EB and selectivity of 93% towards styrene. Other catalysts (CeO₂, ZrO₂ and PH-CeO₂/ZrO₂) show less catalytic activity compared to fluorite CeZrO_{4-δ} catalyst. Fluorite structure of CeZrO_{4-δ} was confirmed by XRD. Presence of Ce⁺³ and Ce⁺⁴ oxidation states and oxygen vacancies of the catalyst favours this ODH reaction, which was supported by the XPS experiment. Fluorite CeZrO_{4-δ} catalyst was stable up to 72 hours time on stream at optimized reaction conditions, which shows approximately 1–2% decrease in conversion and selectivity. The morphology and the structure of the fluorite CeZrO_{4-δ} catalyst were unchanged after 72 hours reaction

which was confirmed by HRTEM and XRD. The fluorite CeZrO_{4-δ} catalyst shows better catalytic activity among the catalysts studied for this particular reaction.

Acknowledgements

TR and KP thanks to SERB-DST (SR/S1/PC-17/2011) for funding.

Notes and references

- 1 R. R. Miller, R. Newhook and A. Poole, *Crit. Rev. Toxicol.*, 1994, **24**, S1–S10.
- 2 E. H. Lee, *Catal. Rev.*, 1974, **8**, 285–305.
- 3 M.-o. Sugino, H. Shimada, T. Turuda, H. Miura, N. Ikenaga and T. Suzuki, *Appl. Catal., A*, 1995, **121**, 125–137.
- 4 Y. Sakurai, T. Suzuki, K. Nakagawa, N.-o. Ikenaga, H. Aota and T. Suzuki, *J. Catal.*, 2002, **209**, 16–24.
- 5 N. R. Shiju, M. Anilkumar, S. P. Mirajkar, C. S. Gopinath, B. S. Rao and C. V. Satyanarayana, *J. Catal.*, 2005, **230**, 484–492.
- 6 P. Kuśtrowski, L. Chmielarz, R. Dziembaj, P. Cool and E. F. Vansant, *J. Phys. Chem. A*, 2004, **109**, 330–336.
- 7 A. K. Venugopal, A. T. Venugopalan, P. Kaliyappan and T. Raja, *Green Chem.*, 2013, **15**, 3259–3267.
- 8 B. M. Reddy, P. Lakshmanan, S. Loidant, Y. Yamada, T. Kobayashi, C. López-Cartes, T. C. Rojas and A. Fernández, *J. Phys. Chem. B*, 2006, **110**, 9140–9147.
- 9 K. Sivarajani, A. Verma and C. S. Gopinath, *Green Chem.*, 2012, **14**, 461–471.
- 10 B. M. Reddy, K. N. Rao, G. K. Reddy, A. Khan and S.-E. Park, *J. Phys. Chem. C*, 2007, **111**, 18751–18758.
- 11 L. Wang, J. J. Delgado, B. Frank, Z. Zhang, Z. Shan, D. S. Su and F.-S. Xiao, *ChemSusChem*, 2012, **5**, 687–693.
- 12 Y. Ohishi, T. Kawabata, T. Shishido, K. Takaki, Q. Zhang, Y. Wang, K. Nomura and K. Takehira, *Appl. Catal., A*, 2005, **288**, 220–231.
- 13 A. Trovarelli, *Catal. Rev.: Sci. Eng.*, 1996, **38**, 439–520.
- 14 J. Kašpar, P. Fornasiero and M. Graziani, *Catal. Today*, 1999, **50**, 285–298.
- 15 H. C. Yao and Y. F. Y. Yao, *J. Catal.*, 1984, **86**, 254–265.
- 16 J. Xu, L.-C. Wang, Y.-M. Liu, Y. Cao, H.-Y. He and K.-N. Fan, *Catal. Lett.*, 2009, **133**, 307–313.
- 17 M. Shen, J. Wang, J. Shang, Y. An, J. Wang and W. Wang, *J. Phys. Chem. C*, 2009, **113**, 1543–1551.
- 18 L. Vivier and D. Duprez, *ChemSusChem*, 2010, **3**, 654–678.
- 19 J. Beckers and G. Rothenberg, *Green Chem.*, 2010, **12**, 939–948.
- 20 E. Aneggi, C. de Leitenburg, G. Dolcetti and A. Trovarelli, *Catal. Today*, 2006, **114**, 40–47.
- 21 M. Pijolat, M. Prin, M. Soustelle, O. Touret and P. Nortier, *J. Chem. Soc., Faraday Trans.*, 1995, **91**, 3941–3948.
- 22 R. Di Monte and J. Kašpar, *Catal. Today*, 2005, **100**, 27–35.
- 23 S. N. Achary, S. K. Sali, N. K. Kulkarni, P. S. R. Krishna, A. B. Shinde and A. K. Tyagi, *Chem. Mater.*, 2009, **21**, 5848–5859.
- 24 I. Atribak, A. Bueno-Lopez, A. Garcia-Garcia and B. Azambre, *Phys. Chem. Chem. Phys.*, 2010, **12**, 13770–13779.

- 25 D. G. Lamas, G. E. Lascalea, R. E. Juarez, E. Djurado, L. Perez and N. E. Walsoe de Reca, *J. Mater. Chem.*, 2003, **13**, 904–910.
- 26 H. Vidal, J. Kašpar, M. Pijolat, G. Colon, S. Bernal, A. Cordón, V. Perrichon and F. Fally, *Appl. Catal., B*, 2000, **27**, 49–63.
- 27 B. Reddy, P. Bharali, G. Thrimurthulu, P. Saikia, L. Katta and S.-E. Park, *Catal. Lett.*, 2008, **123**, 327–333.
- 28 B. Reddy and A. Khan, *Catal. Surv. Asia*, 2005, **9**, 155–171.
- 29 D. Zhao, J. Sun, Q. Li and G. D. Stucky, *Chem. Mater.*, 2000, **12**, 275–279.
- 30 A. Pfau and K. D. Schierbaum, *Surf. Sci.*, 1994, **321**, 71–80.
- 31 L. Jiang, H. Zhu, R. Razzaq, M. Zhu, C. Li and Z. Li, *Int. J. Hydrogen Energy*, 2012, **37**, 15914–15924.
- 32 F. Zhang, P. Wang, J. Koberstein, S. Khalid and S.-W. Chan, *Surf. Sci.*, 2004, **563**, 74–82.
- 33 A. Bensalem, F. Bozon-Verduraz, M. Delamar and G. Bugli, *Appl. Catal., A*, 1995, **121**, 81–93.
- 34 A. Galtayries, R. Sporcken, J. Riga, G. Blanchard and R. Caudano, *J. Electron Spectrosc. Relat. Phenom.*, 1998, **88–91**, 951–956.
- 35 A. E. Nelson and K. H. Schulz, *Appl. Surf. Sci.*, 2003, **210**, 206–221.
- 36 H. Xu, D.-H. Qin, Z. Yang and H.-L. Li, *Mater. Chem. Phys.*, 2003, **80**, 524–528.
- 37 K. N. Rao, B. M. Reddy, B. Abhishek, Y.-H. Seo, N. Jiang and S.-E. Park, *Appl. Catal., B*, 2009, **91**, 649–656.
- 38 T. M. Sankaranarayanan, R. H. Ingle, T. B. Gaikwad, S. K. Lokhande, T. Raja, R. N. Devi, V. Ramaswamy and P. Manikandan, *Catal. Lett.*, 2008, **121**, 39–51.